# Experimental Study on the Local Turbulence Modulation in a Horizontal Particle Laden Flow with Rigid Fence

**Fusheng Yang*†, Daisuke Aoshima*, Kenji Otakeguchi*, Takahiro Tsukahara*, Yasuo Kawaguchi***

* Department of Mechanical Engineering, Tokyo University of Science, Noda, Japan
† Department of Process Equipment and Control Engineering, Xi'an Jiaotong University, Xi'an, China

**Abstract.** The turbulence modulation by the existence of disperse phases, e.g. solid particles or liquid droplets, has attracted wide attentions in recent years. In this investigation, particles of different properties were fed with tracers into the turbulent atmospheric boundary layer disturbed by a rigid fence, and the velocities of both phases were obtained by PIV/ PTV methods respectively. From both ensemble average and instantaneous analysis, the presence of particles was found to attenuate the local turbulence around the fence and in the downstream. In this case, the induced sand dune erosion by the turbulence when installing the rigid fence is also expected to decrease. The influences of the particles follow the order: GH>GL>No.9. The Stokes number under the given conditions showed that all the particles under discussion should cause augmented dissipation of turbulence. Moreover, through analyzing the relative velocities between the two phases, the cross-trajectory effect was found to be another possible mechanism accounting for the observed turbulence modulation by the particles.

## INTRODUCTION

The interaction between the dispersed and continuous phases in turbulent regime represents a common interest in the two-phase flow studies, and thus many researchers have investigated it experimentally or numerically. Elghobashi[1], Growe et al.[2] reviewed the modeling techniques for turbulent two phase flow, in which a few characteristic parameters (e.g. volumetric fraction of particles, time scale ratio between particle and turbulence) were recommended as the criteria to qualitatively evaluate the turbulence modulation. Best et al. [3] conducted PDA experiments on the water flow over flat sand bed, and the existence of mobile particles was found to enhance the turbulent intensity near the bed, yet suppress it in the upper region. Sato et al. [4] explored the turbulent distortion around particles in a vertical channel flow using DPIV method, and their results proved the impact of particle spacing on the enstrophy production. In a DNS simulation study on the vertical channel flow, Kajishima et al. [5] found that the wakes from the particles strongly affect the velocity and vorticity fluctuations, as well as the Reynolds shear stress. Nezu and Azuma [6] utilized PTV method to simultaneously measure the velocities of solid and liquid phases in an open channel flow, and substantial turbulence enhancement was observed in the vicinity of the surface due to the particle movement. Mergheni et al. [7] carried out experimental study on a vertical coaxial jet by PDA, from which the existence of particles was observed to reduce the velocity gradient in the shear layer, causing a decrease in turbulence intensity. In the recent simulation studies [8, 9], the turbulence enhancement by large particles, as well as the turbulence attenuation by small particles have both been successfully predicted in a unified model by appropriate numerical settings.

Nowadays, it is generally accepted that "large" particles tend to enhance turbulence by vortex shedding, while "small" particles lead to intensive dissipation and attenuation in turbulence. Nevertheless, it should be pointed out that quite a few mechanisms link to the turbulence modulation by particles [3, 10], hence the abovementioned criteria is far from sufficient to completely explain such effects in all practical cases. Therefore, more experimental work is still necessary or even imperative for the basic understanding of the phenomena, especially on the relatively complicated flow field.

In our previous work, the turbulent flow around a small-size fence with different porosities, as well as its effects on sand dune erosion, have been investigated by multiple laser-based techniques [11]. Through laser visualization the sand dune shape was recorded continuously, and a 30% porosity fence was found most effective in suppressing the turbulence-induced sand erosion. The relatively small turbulent intensity around the dune crest will account for this result. As an extension of the study, a series of wind tunnel experiments were conducted for the turbulent flow

around a similar rigid fence in this investigation, in hope of further elucidating the 2-way or even 4-way coupling mechanism in the flow field. Note that due to the addition of fence, the distribution pattern of particles is changed from 1-D to 2-D, under which condition the discussion of inter-phase effects in local region becomes important. Using oil mist as flow tracers, the simultaneous measurement of velocities for both gas and solid phases was made, PIV and PTV methods were applied respectively to extract their velocities. Thereafter, the single phase flow field and the two-phase flow fields with different particles were compared, and the effects of particle motions on the local turbulent flow were analyzed in combination with the relative velocity between two phases. The results of this work are expected to improve our understanding about the turbulent modulation by particles with different properties.

## EXPERIMENTAL SET-UP AND DATA PROCESSING

### Wind Tunnel Apparatus

The experimental set-up is shown in Fig. 1. The blower and rectification section was 2910mm long, and its internal dimension at the end was $250\times250mm^2$. The developing section was 1000mm long, the test section was 3000mm long, and the spanwise width of each section was 250mm. The wind tunnel was designed to eliminate pressure gradient as possible, and the wind velocity can be adjusted from 0 to 20m/s. Roughness blocks were installed in the developing section to generate turbulence, and the minimum intensity was about 0.5%.

In this investigation, three kinds of particles with different size and density, namely No.9 sand particles, GL and GH glass particles were used in the experiments, and their detailed properties were given in Table.1. The olive oil mist of 1~3μm diameter was utilized as the fluid tracers, and its density was $833kg/m^3$. The particle Reynolds number for the tracer was calculated to be around $10^{-5}$, thus the tracer should be able to follow the flow very well. The particles were supplied continuously using a piston-type feeding device installed at the upstream of test section, as shown in Fig. 1. A detailed description of the feeding device is referred in Otakeguchi et al. [12]. In the test region, a small fence of 20mm height was installed, and the concerning turbulent flow field around it could be observed.

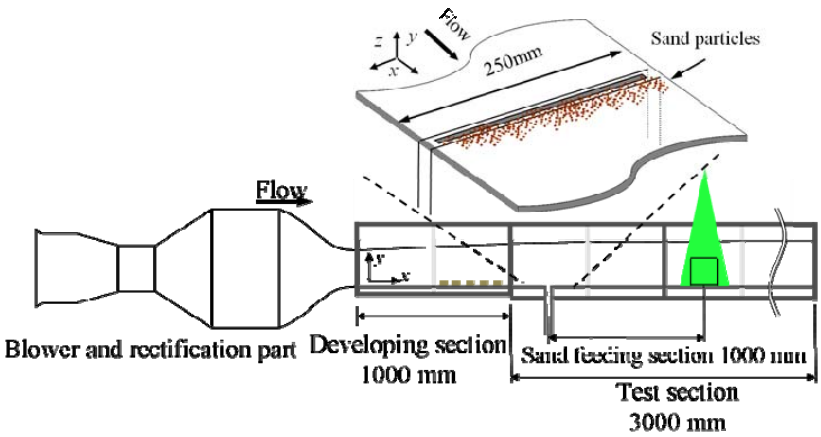


**FIGURE 1.** The experimental set-up

**TABLE 1.** Properties of the particles

| Index | Material | Density ($kg/m^3$) | Median diameter (μm) | Standard deviation of particle diameter (μm) |
|---|---|---|---|---|
| No.9 | Sand | 2560 | 50.4 | 61.9 |
| GL | Glass | 2500 | 111 | 19.7 |
| GH | Glass | 4200 | 108 | 19.9 |

## Image Data Acquisition and Processing

The image data of both phases were collected using a PIV measurement system, which was composed of a double-pulse laser, laser-sheet optics arrangement, CCD camera, synchronizer, and a PC for data processing.

The double-pulse laser (Litron Laser, Co.: Nano S 65-15) was a combination of a pair of Nd: YAG lasers, each having an output of 40mJ/pulse and a wavelength of 532nm. The pulse interval was set as 50μs. The laser sheet thickness and the spread angle were set as 0.6mm and 20°, respectively. The CCD camera had a resolution of 2048 $\times$2048pixels, the pixel pitch was 7.4$\times$7.4μm, and the field of view (FOV) was 112$\times$112mm$^2$. The lens had a focal length of 50mm and aperture of 2.8.

When enough image data (for each setting at least 600 sets) were collected, we exported them from the PIV software (Dantec dynamics Co.: Dynamic Studio 2.30). Thereafter, one image with both phases was processed using home-made program, from which two images with individual phases were generated. The procedure was based on the intensity and size threshold of the sand particles, as elaborated in Aoshima et al. [13]. For the image series of tracer images, the commercial PIV software mentioned above was utilized for the flow field calculation, based on a multi-step adaptive correlation procedure. The velocity vectors out of certain range or obviously inconsistent with surrounding vectors were rejected and substituted. On the other hand, the image series of the dispersed phase, i.e. sand particles were processed by a particle tracking velocimetry (PTV) procedure, generating the particle velocities. A bidirectional relaxation algorithm proposed by Zhang et al. [14], which proved to have good performance in processing image pair with numerous isolated non-matching particles, was adopted in our program. Firstly each particle centroid was determined by a Gaussian digital mask [15] for all the image frames, and then particles in the first frame were matched with those in the second frame by the iterative relaxation method [16]. For the so-called bidirectional algorithm, a reverse matching process from the second frame to the first one is added to increase the probability of correct matching. From the free stream velocity of the air flow, the maximum particle displacement was estimated to be around 10 pixels within the time interval of 50 μs, thereby the movement threshold $T_m$ of the algorithm was specified as 12pixels to guarantee the vector recovery ratio. The specification of the neighborhood threshold $T_n$ and semi-rigidity threshold $T_p$, which were also related to the maximum displacement, followed the recommendations for good performance by Baek and Lee [16]. The free stream velocity $U_\infty$ is 9.5m/s on condition that no fence is installed.

# RESULTS AND DISCUSSION

## Ensemble Average Flow Field

The ensemble mean streamwise velocity and the Reynolds shear stress of the clear air flow are shown in Fig. 2(a) and (b), respectively. These flow parameters were normalized by the freestream velocity $U_\infty$, while the dimension of the FOV was normalized by the size of the fence $h_f$. In the upstream the flow field is similar to that without the fence, except that the velocity gradient d$U$/d$y$ shows minor increase towards the fence. On the other hand, a significant velocity gradient can be observed in the near downstream of the fence tip, suggesting strong shear effects and active turbulence generation. From Fig. 2(b) we find two regions with large Reynolds shear stress, one is around the fence tip (named Region a) and the other locates in the downstream of the fence (name Region b). Relatively strong turbulence fluctuation is expected in these regions.

As pointed out by Zhang et al. [17], the ensemble averaging of the flow fields laden with particles does not mean that the two-phase flow is steady, instead it just provides some means to evaluate the general effect of particles on the flow. For the turbulent flow laden with No.9, GL and GH particles, the mean streamwise velocity and Reynolds shear stress in the FOV were shown in Fig. 3-5, respectively.

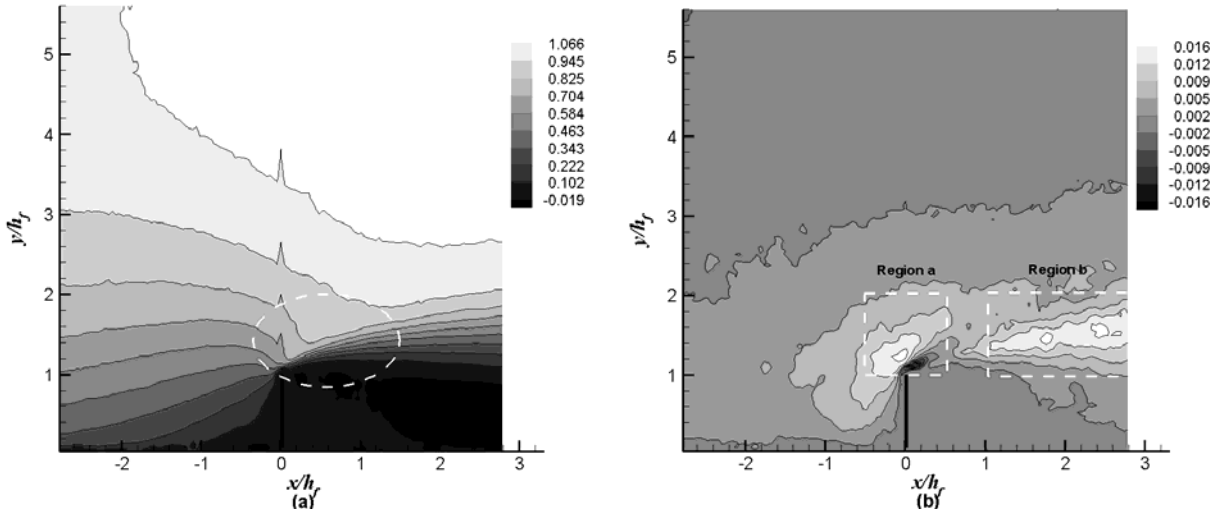


**FIGURE 2.** The clear air flow field: (a) Ensemble mean streamwise velocity; (b) Reynolds shear stress

The influence of No.9 particles on the mean flow field is relatively weak from Fig. 3(a). In the upstream of the fence almost no difference can be found compared with Fig. 2(a), while the local velocity contours near the fence tip move towards up-right direction a little, suggesting reduced velocity gradient and shear effect. From Fig. 3(b) the local Reynolds shear stress around the fence tip decreases down to about 0, yet such attenuating effect is much less pronounced in the far downstream region.

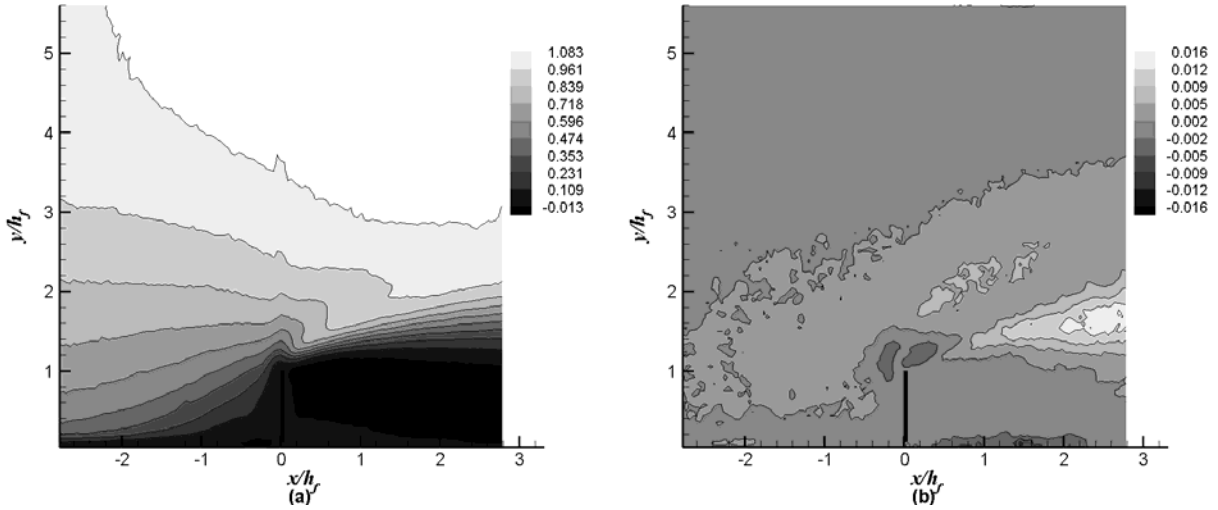


**FIGURE 3.** The flow field with No.9 particles: (a) Ensemble mean streamwise velocity; (b) Reynolds shear stress

GL particles exert larger influences on the flow, as can be seen in Fig. 4(a). In the upstream of the fence, the low velocity region near the surface expands and the local velocity gradient d$U$/ d$y$ there decreases, as found for the two phase flow without the fence [12]. The more remarkable difference appears in the near downstream of fence tip, where the spacing between the initially crowded velocity contours gets larger. On the other hand, from Fig. 4(b) the Reynolds shear stress around the fence tip becomes negative, which means that the particles may change the nature of the turbulence. In addition, more significant turbulence attenuation compared to No.9 particles can be found in the far downstream of the fence.

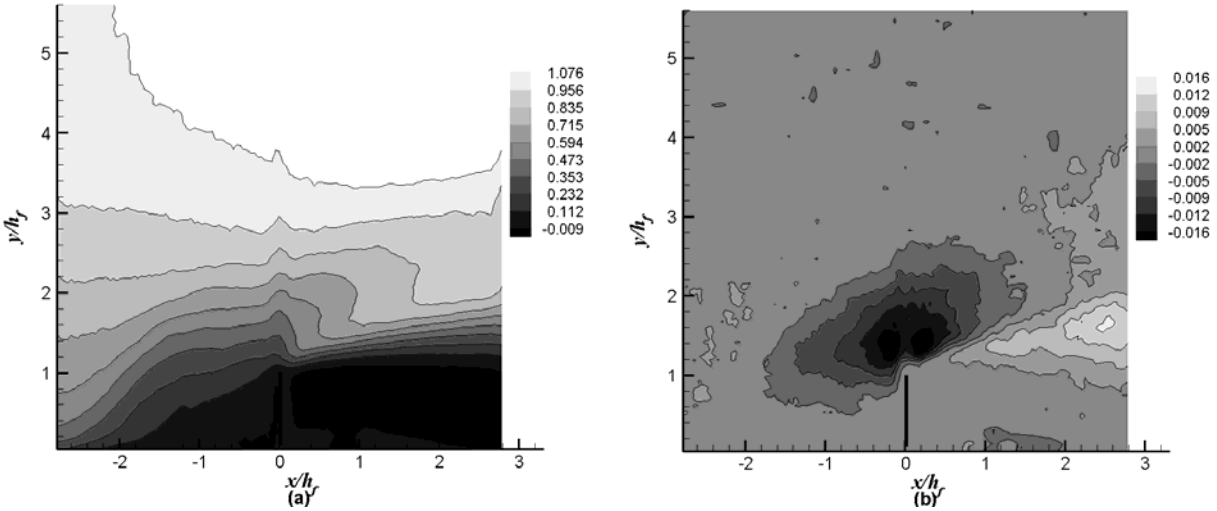


**FIGURE 4.** The flow field with GL particles: (a) Ensemble mean streamwise velocity; (b) Reynolds shear stress

As shown by Fig. 5, the influences of GH particles on the flow are qualitatively similar to those by GL particles, yet the influencing area is even larger and the effects are stronger.

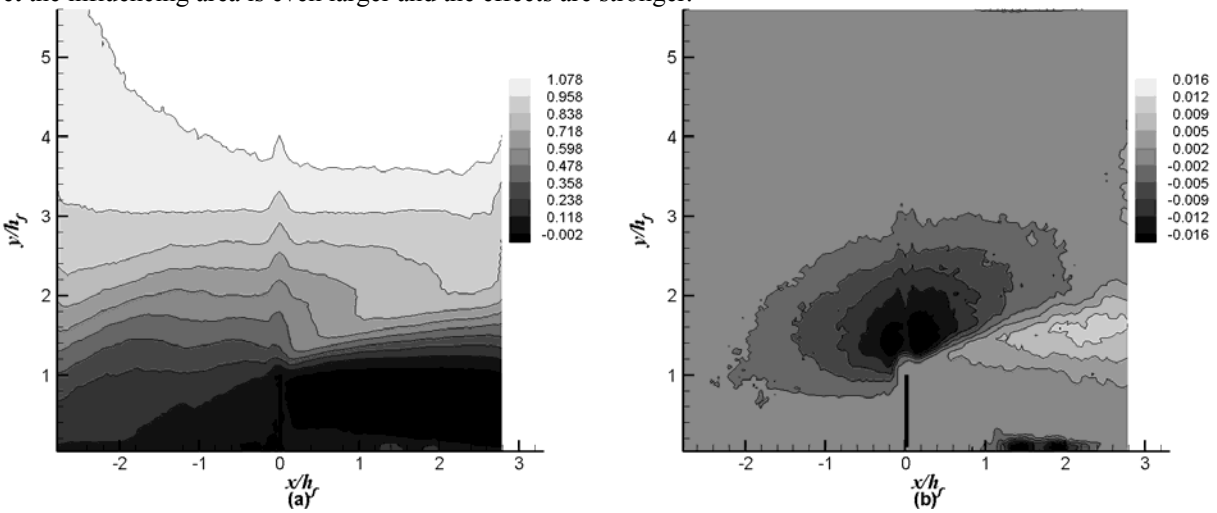


**FIGURE 5.** The flow field with GH particles: (a) Ensemble mean streamwise velocity; (b) Reynolds shear stress

From the above results we can see that for all the types of particles under discussion, the modulation effects on the turbulence seem to be different in region a and b, hence the discussion will be conducted respectively for them.

## Temporal Variations of Particle Concentration and Turbulence Intensity

Although the flow in the whole FOV should be turbulent, our interest focuses on the turbulence generated from the fence tip, which was found responsible for the intensive sand dune erosion in the downstream [11]. In this investigation, we also confirm the strong turbulence in the downstream of fence, see the swirling strength $\lambda$ for a typical instantaneous flow field without particles in Fig. 6. The swirling strength, which characterizes the rotating motion of turbulence, was calculated and normalized by the characteristic time scale [11]. When the particles are present in the flow, the swirling strength tends to decrease in the downstream of the fence. It is noteworthy that the mass loading of the flow varies temporarily, thus the abovementioned attenuating effect is also varied. To explore such effect in more detail, the instantaneous particle concentration and swirling strength, which were the average results in the local regions a and b, were compared in the whole time span, see Fig. 7-9.

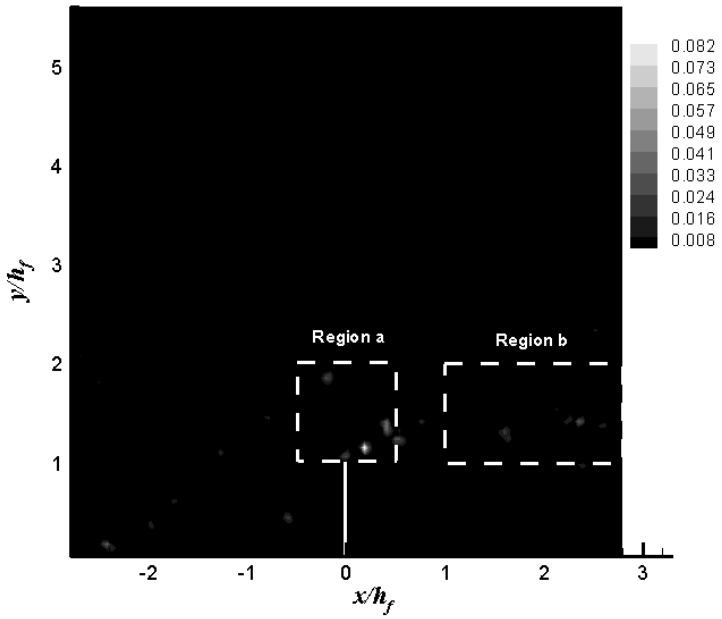


**FIGURE 6.** The swirling strength of typical instantaneous clear air flow field

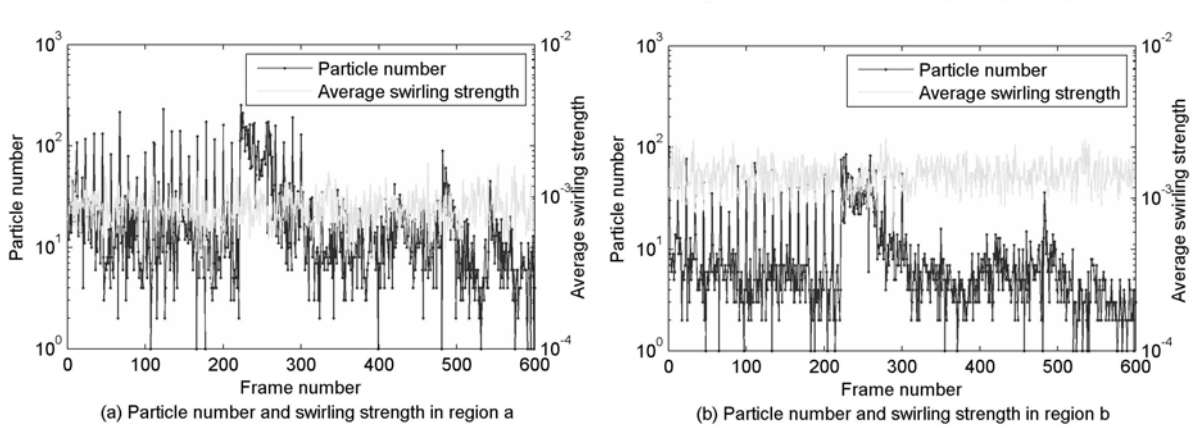


**FIGURE 7.** The temporal variations of particle number and average swirling strength in region a and b (No.9 particles)

For No.9 particles, we can see that the correlation between particle presence and turbulence intensity is relatively weak in a certain region, the swirling strength $\lambda$ appears to fluctuate around the temporally-averaged value in an irregular manner. However, it should be noted that in region a, where more particles are present than in region b, the magnitude of fluctuation in $\lambda$ is generally larger. Moreover, on average the swirling strength in region a also shows relatively small value. This comparison result indirectly proves that the existence of No.9 particles actually reduces the local turbulent motion. Nevertheless, such effect is not so strong that can be clearly discriminated from the essential fluctuation of turbulence. On the other hand, as is found in Fig. 8 and 9, the swirling strength fluctuates in a wider range when GL and GH particles are present instead of No.9 particles, suggesting more remarkable influences. We can see as the number of glass particles increases, generally a decrease in $\lambda$ can be observed at the same time. A local maxima of the particle number $N$ corresponds to a local minima of swirling strength $\lambda$, and vice versa. Besides, due to the larger number of particles in region a than in region b, the temporally-averaged swirling strength in region a is smaller, with a larger fluctuation, which is similar to the phenomena in the case of No.9 particles. However, the difference in particle number between region a and b is not so large for GL and GH particles as for No.9 particles, hence the turbulence modulation effects in region a and b show less significant difference for glass particles.

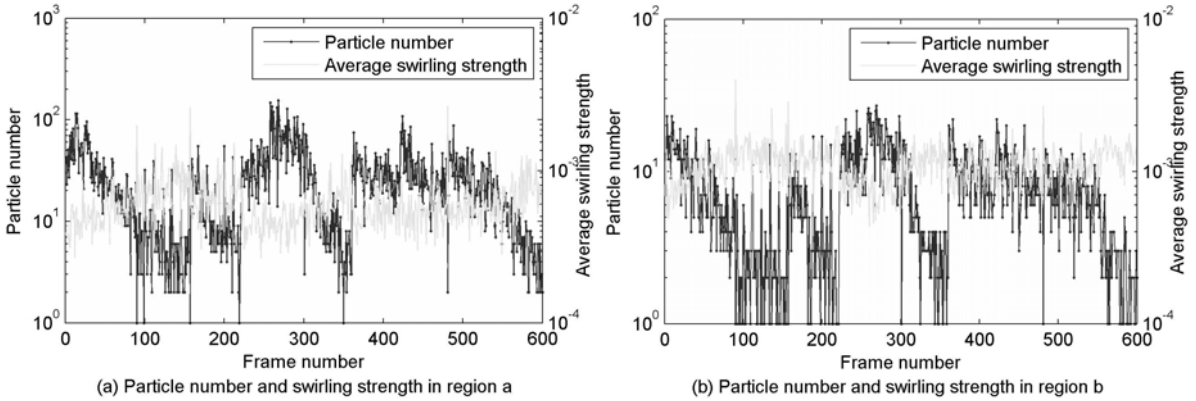


**FIGURE 8.** The temporal variations of particle number and average swirling strength in region a and b (GL particles)

To further testify the above conclusion, an analysis based on the correlation coefficient defined in Eq. (1) was carried out.

$$c(\lambda, N) = \overline{\lambda' \cdot N'} / \left( \overline{\lambda'^2} \cdot \overline{N'^2} \right)^{1/2} \tag{1}$$

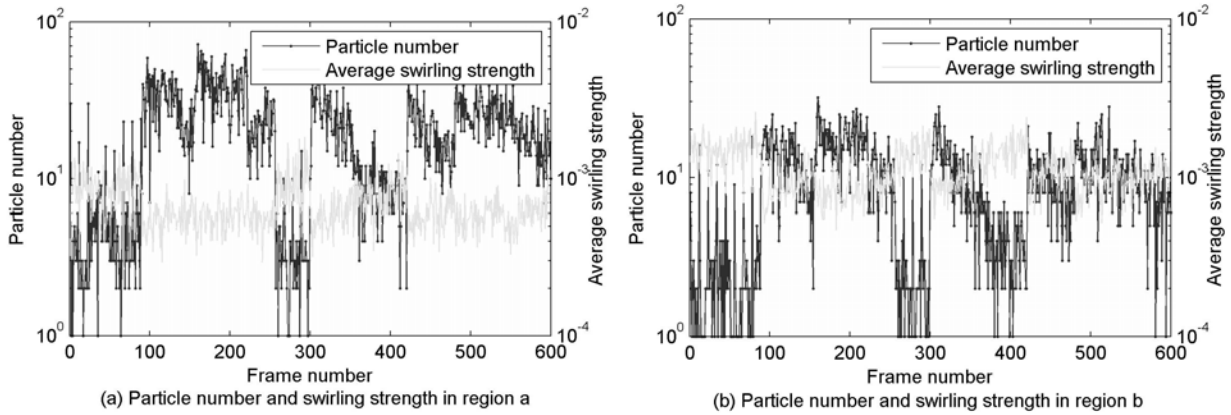


**FIGURE 9.** The temporal variations of particle number and average swirling strength in region a and b (GH particles)

In the case of No.9 particles, the correlation coefficients between particle number and swirling strength in region a and b are around 0.5, while these values increase up to 0.6 or higher for GL and GH particles. In summary, the turbulence modulation effects from the various particles are qualitatively similar (attenuation), while the magnitudes follow the order: GH> GL> No.9. As a result, the induced sand dune erosion in the downstream of the fence should also decrease when the coming flow is laden with particles under discussion.

For the isotropic turbulence, the effects of particles on turbulence intensity are generally explained by the vortex shedding or augmented dissipation. The effect of particles on the turbulence is always evaluated using Stokes number, which is the ratio of particle response time to the flow time scale.

The particle response time was calculated following Taniere et al. [18],

$$\tau_p = \rho_p d_p^{\,2} / \left( 18\mu \left( 1 + \mathrm{Re}_p^{0.687} \right) \right) \tag{2}$$

For the No.9, GL and GH particles, the values were obtained as 0.0092, 0.0312 and 0.0503s from the particle properties listed in Table 1.

For the horizontal turbulent flow in the atmospheric boundary layer (ABL), the largest time scale of flow can be expressed as follows:

$$\tau_L = \frac{\delta}{0.1U_\infty} \tag{3}$$

According to our previous work [12], the boundary layer thickness under the present experimental conditions is around 90mm, which should be good enough to be used as a rough estimate. The Stokes number defined as $\tau_p/\tau_L$ in the case of different particles can be calculated as 0.097, 0.33 and 0.53. It is noted that due to the temporally varying mass loading, the full turbulence development in the downstream can hardly be achieved, hence the size of large eddy may be smaller than the boundary layer thickness. In other words, $\tau_L$ may be actually smaller than calculated, resulting larger *St*. Anyway, the criterion of augmented dissipation by the particles ($St_L$<1) according to Elghobashi [1] seems able to be satisfied, which could at least partly explain the turbulence suppression by particles.

## Relative Velocity and Inter-phase Effects

According to Best et al. [3], the particles may affect turbulence strength through many mechanisms, such as varying surface roughness, crossing trajectory effect by inertia, vortex shedding and interfering with the local turbulent structures. Therefore, the above explanation of turbulence modulation in section 3.2 may not be complete and further analysis should be necessary. Considering that relative velocities between particles and surrounding fluid are important for characterizing the inter-phase effects, they were calculated in the region a and b. In addition, the angle between the velocity vectors of both phases α was also obtained. The joint PDFs of relative velocity components, i.e. $U_p - U_g$, $V_p - V_g$, as well as the PDFs of the angle α, were given in Fig. 10-12 for the cases with No.9, GL and GH particles. Since the fluid velocities were evaluated in a uniform grid by PIV method, an interpolation procedure based on the inverse distance was applied to extract the fluid velocity at the position of particles. In region a and b, more than 10000 and 4000 data samples were collected for the abovementioned statistical analysis, respectively.

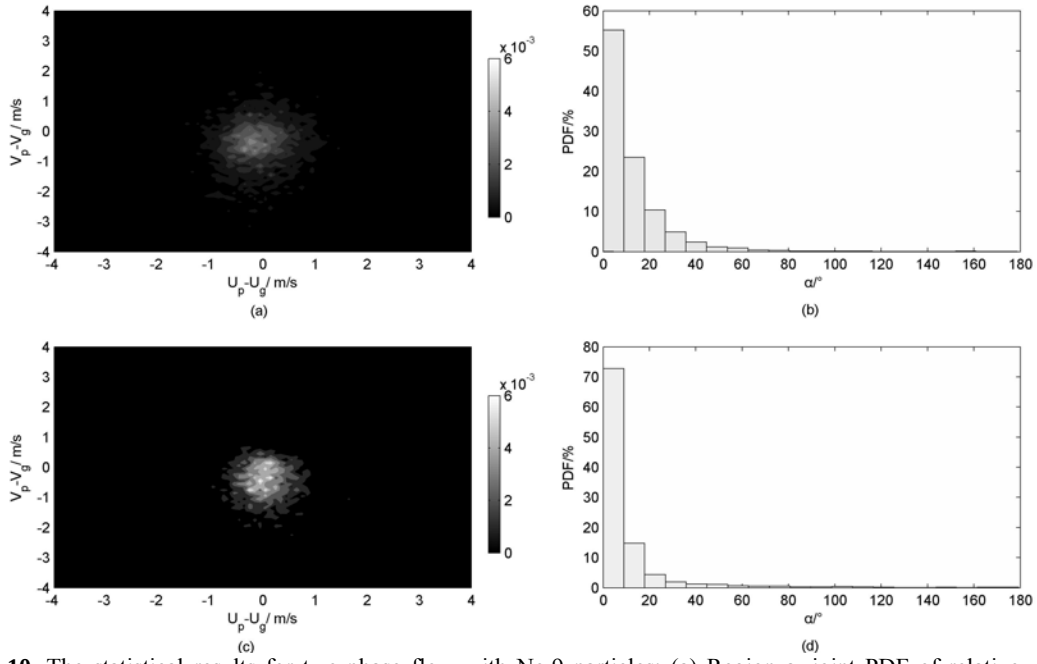


**FIGURE 10.** The statistical results for two-phase flow with No.9 particles: (a) Region a, joint PDF of relative velocity; (b) Region a, PDF of angle; (c) Region b, joint PDF of relative velocity; (d) Region b, PDF of angle

Figure 10 shows that for No.9 particles in region a, the distribution of $U_p - U_g$ and $V_p - V_g$ is fairly uniform and symmetric around the origin, and no obvious gradient can be observed. The angle between the velocities of both phases mostly concentrates in a small range below 20°, suggesting weak cross-trajectory effects. On the other hand, in region b the distribution area of relative velocity on the plane shrinks, while the peak of PDF curve of angle $\alpha$ is shifted towards 0. Because of the drastic change of flow direction in region a due to the installation of fence, the particles are more difficult to follow the flow, resulting in large relative velocity and angle.

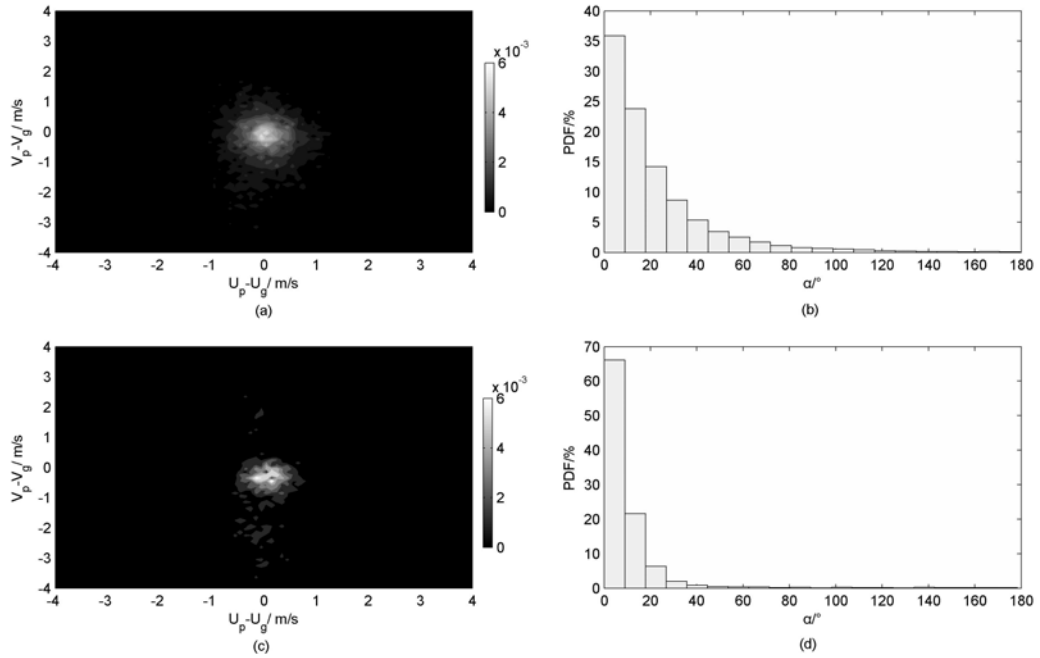


**FIGURE 11.** The statistical results for two-phase flow with GL particles: (a) Region a, joint PDF of relative velocity; (b) Region a, PDF of angle; (c) Region b, joint PDF of relative velocity; (d) Region b, PDF of angle

From Fig.11, for GL particles in region a, the distribution of relative velocity components is less regular compared to No.9 particles, and the probability decreases gradually outwards, with a sharp peak at the origin. The distribution of $\alpha$ is more scattered towards the large value, thus stronger cross-trajectory effect could be expected. In region b, the joint PDF of relative velocity components is narrow along $x$-axis, and the significant effect of gravity can be confirmed from the obvious extension towards negative value in $y$-direction. Another noteworthy fact is that in region b, where the flow is relatively calm and steady, the PDF curve of $\alpha$ for GL particles shows little difference compared to that for No.9 particles. This means that only in the region with strong flow event, the different properties of particles under discussion will be important in the aspect of flow modulation.

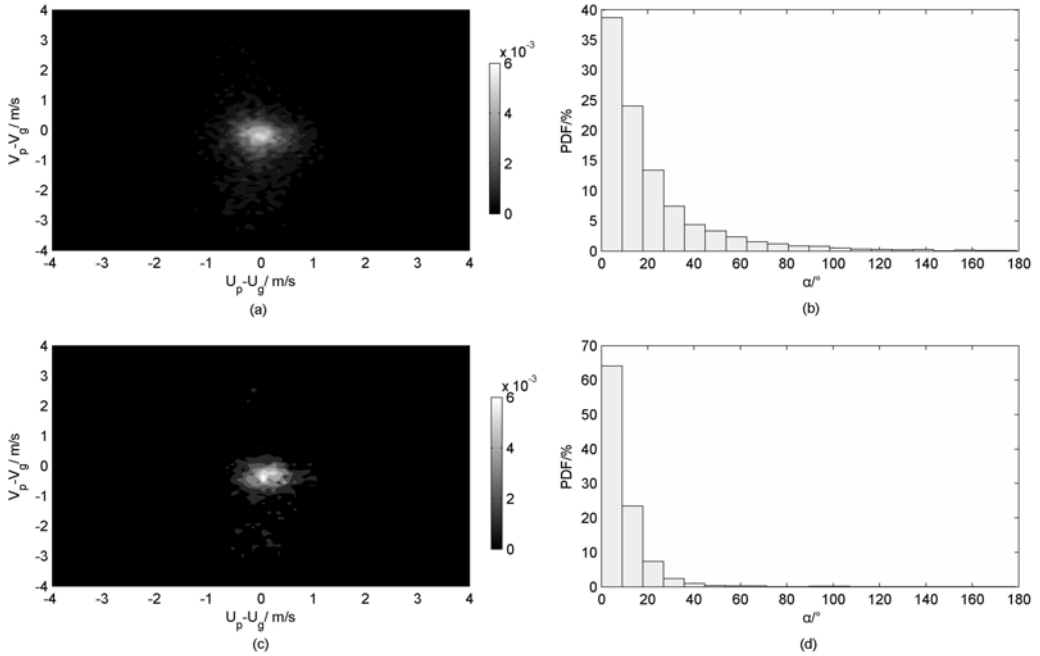


**FIGURE 12.** The statistical results for two-phase flow with GH particles: (a) Region a, joint PDF of relative velocity; (b) Region a, PDF of angle; (c) Region b, joint PDF of relative velocity; (d) Region b, PDF of angle

The statistical characteristics for the flow with GH particles are qualitatively similar to those with GL particles, see Fig. 12. However, some small difference can still be observed. For example, due to the larger density of particles, even in region a, the strong effect of gravity leads to the preference of joint PDF towards negative value of $V_p - V_g$, which is less remarkable in Fig.11(a).

## CONCLUSION

Through analyzing the image data collected from a series of wind tunnel experiments, the influences of different particles on the turbulence generated by a rigid fence installed in the simulated atmospheric boundary layer were investigated. The following conclusions can be drawn:

1) The presence of particles generally reduces the local turbulence intensity, the magnitude of effects follows the order: GH> GL> No.9.

2) In the region near the fence tip, the turbulence modulation effect is stronger than that in the downstream.

3) According to the Stokes number calculation, all the three particles augment the turbulence dissipation.

4) GL and GH particles show greater cross-trajectory effect in region a, which may explain their more significant turbulence modulation compared to No.9 particles.

## REFERENCES


1. S. Elghobashi, Applied Scientific Research **52**, 309-329 (1994).
2. C.T. Crowe, T.R. Troutt, J.N. Chung, Annu. Rev. Fluid Mech. **28**, 11-43 (1996).
3. J. Best, S. Bennett, J. Bridge, M. Leeder, J Hydraulic Engineering **123**, 1118-1129 (1997).
4. Y. Sato, U. Fukuichi, K. Hishida, Int. J Heat and Fluid Flow **21**, 554-561 (2000).
5. T. Kajishima, S. Takiguchi, H. Hamasaki, Y. Miyake, JSME International Journal(Series B) **44**, 526-535 (2001).
6. I. Nezu and R. Azuma, J Hydraulic Engineering **130**, 988-1001 (2004).
7. M. Mergheni, H. Ben Ticha, J. Sautet, G. Godard, S. Ben Nasrallah, Thermal Science **12**, 59-68 (2008).
8. M. Mandø, M.F. Lightstone, L. Rosendahl, C. Yin, H. Sørensen, Int. J Heat and Fluid Flow **30**, 331-338 (2009).
9. N. Alvandifar, M. Abkar, Z. Mansoori, M. Saffar Avval, G. Ahmadi, Int. J Heat and Fluid Flow **32**, 826-833 (2011).
10. A.W. Vreman, J. Fluid Mech. **584**, 235-279 (2007).
11. T. Tsukahara, Y. Sakamoto, D. Aoshima, M. Yamamoto, Y. Kawaguchi, Experiments in Fluids **52**, 877-890 (2012).
12. K. Otakeguchi, D. Aoshima, Y. Sakamoto, T. Tsukahara, Y. Kawaguchi, M. Yamamoto, Proc. ASME-JSME-KSME Joint Fluids Engineering Conference, Shizuoka, Japan, 2011.
13. D. Aoshima, K.Otakeguchi, Y.Sakamoto, T.Tsukahara, M. Yamamoto, Y. Kawaguchi, 2011. Proc. 9th Int. Symp. on Particle Image Velocimetry- PIV'11, Tsukuba, Japan, 2011.
14. Y. Zhang, Y. Wang, Z.Q. Li, ACTA AERODYNAMICA SINICA (in Chinese) **28**, 250-254 (2010).
15. I.F. Sbalzarini and P. Koumoutsakos, J Structural Biology **151**, 182-195 (2005).
16. S.J. Baek and S.J. Lee, Experiments in Fluids **22**, 23-32 (1996).
17. W. Zhang, Y. Wang, S.J. Lee, Experiments in Fluids **45**, 241-256 (2008).
18. A. Taniere, B. Oesterle, J.C. Monnier, Experiments in Fluids **23**, 463-471 (1997).